Archiv der Pharmazie

DPhG

FULL PAPER

Design, Synthesis, and Biological Evaluation of Novel Benzimidazole/Schiff Base Hybrid Derivatives With Potential Biological Activities

Mohamed Y. Abdel-Hady[1] | Martha M. Morcoss[2] | Abdullah Yahya Abdullah Alzahrani[3] | Bahaa G. M. Youssif[4] | El Shimaa M. N. Abdelhafez[5] | Mohamed Abdel-Aziz[5]

[1]Pharmaceutical Chemistry Department, Faculty of Pharmacy, Badr University in Assiut (BUA), Asyut, Egypt | [2]Department of Pharmaceutical Chemistry, Faculty of Pharmacy, Nahda University, Beni-Suef, Egypt | [3]Department of Chemistry, Faculty of Science, King Khalid University, Abha, Saudi Arabia | [4]Pharmaceutical Organic Chemistry Department, Faculty of Pharmacy, Assiut University, Assiut, Egypt | [5]Department of Medicinal Chemistry, Faculty of Pharmacy, Minia University, Minia, Egypt

Correspondence: Bahaa G. M. Youssif (bgyoussif2@gmail.com) | Mohamed Abdel-Aziz (Abulnil@hotmail.com)

Received: 5 August 2025 | **Revised:** 4 November 2025 | **Accepted:** 25 November 2025

Keywords: antiproliferative | benzimidazole | EGFR | HER-2 | hydrazone | thiosemicarbazide

ABSTRACT

A novel series of benzimidazole-based derivatives **(5a–g)**, **(6a–b)**, and **(7a–b)** were designed, synthesized, and evaluated for their potential as dual inhibitors of EGFR and HER-2. The synthesized compounds were subjected to in vitro screening against a panel of selected human cancer cell lines. Additionally, their cytotoxicity was assessed using normal human mammary epithelial cells (MCF-10A) to evaluate their safety profile. Among the tested derivatives, compounds **5b, 5f**, and **6a** demonstrated the most pronounced antiproliferative activity, exhibiting IC_{50} values of 6, 8, and 5 μM, respectively. These values reflect a potency at least fourfold greater than that of the reference drug Doxorubicin ($IC_{50} = 33$ μM). EGFR and HER-2 enzyme inhibition assays were conducted to explore the potential molecular targets responsible for the observed anticancer effects. Notably, compound **6a** (R_1 = phenyl, thiosemicarbazide) exhibited superior efficacy against the MCF-7 breast cancer cell line, with an IC_{50} of 5 μM, approximately six times more potent than Doxorubicin. Conversely, compound **7b**, with an IC_{50} value of 85 μM against MCF-7 cells, was the least active, underscoring the critical role of the phenyl moiety in antiproliferative activity. Furthermore, a molecular docking study was conducted to investigate the binding interactions of **6a** within the active sites of EGFR and HER-2, providing insight into its potential mechanism of action.

1 | Introduction

Cancer is classified as one of the most aggressive and fatal diseases globally. GLOBOCAN 2021 estimates indicate that in 2020, there were approximately 18.1 million new cancer diagnoses and 9.6 million cancer-related deaths globally [1]. Female breast cancers have overtaken lung cancers as the most often diagnosed malignancies, with an anticipated 2.3 million new cases (11.7%), followed by lung cancers (11.4%) and colorectal cancers (10.0%). Lung cancer continued to be the predominant cause of cancer mortality, accounting for over 1.8 million fatalities (18%) [2]. Targeted therapy, a distinctive form of chemotherapy, effectively inhibits the proliferation and dissemination of cancer cells by focusing on certain genes or proteins.

The epidermal growth factor receptor (EGFR) family, comprising EGFR (ErbB1, HER1), HER-2 (ErbB2), HER3 (ErbB3), and HER4 (ErbB4), is a prominent subfamily of protein kinases, commonly referred to as HER or ErbB receptors [3, 4]. The EGFR family is crucial in signal transduction, and its overexpression is associated with the etiology of various human solid tumors, including non-small cell lung cancers (NSCLCs)

and breast cancers [5–7]. EGFR inhibitors are commonly used to treat breast and NSCLCs cancers by inhibiting the EGFR-controlled signaling pathways.

Cancer is a complicated disease; thus, targeting a single cause may result in treatment failure [8–10]. In general, the EGFR kinase inhibitors used in clinical settings only worked when cancer cells had certain EGFR mutations that made them more likely to be activated. These mutations seemed to keep the ligand-dependency of receptor activation while changing the signaling patterns further downstream [11]. A limited percentage of lung cancer patients may derive benefits from treatment with EGFR inhibitors [12]. Cancers that initially respond to treatment with EGFR inhibitors frequently develop resistance due to point mutations in the ATP-binding site of EGFR, including T790M, L858R, and Cys797, among others [13, 14]. Moreover, cancer cells may activate specific pro-survival signaling pathways, as demonstrated by the amplification of MET in lung tumors subjected to EGFR inhibitors [15, 16].

Combination therapy that targets many cancer pathways has demonstrated efficacy through synergistic and/or additive methods. The simultaneous administration of many medications remains a barrier in clinical therapy due to numerous dose-limiting toxicities and drug–drug interactions resulting from modified pharmacokinetic profiles [17, 18]. Consequently, a singular pharmaceutical agent aimed at two or more targets may constitute an efficacious approach for cancer treatment. Currently, medications exhibiting poly-pharmacological activities demonstrate greater advantages over combination therapy due to their reduced incidence of adverse effects and enhanced therapeutic resilience [19]. The dual target-single-agent approach has emerged as a prominent area of research in cancer treatment, with increasing interest among researchers in developing innovative dual-target drugs in recent years. A multitude of research examining the efficacy of dual or multi-target inhibitors targeting wild-type and/or mutant EGFR have been accomplished yielding promising results that suggest these inhibitors represent an appealing way to enhance anticancer activity and/or surmount drug resistance [9, 20–23].

HER-2 and EGFR, as members of the EGFR family, exhibit the highest homology in their kinase catalytic domains and share multiple analogous biochemical and kinetic characteristics. Aberrant expression of HER-2 is crucial in the advancement of numerous aggressive malignancies, including breast cancers and NSCLCs [24, 25]. Furthermore, its overexpression may enhance glucose uptake, oxygen consumption, and lactate generation, leading to the reprogramming of tumor metabolism [26]. The utilization of multiple HER-2 inhibitors in cancer treatment suggests with the synergistic transformative effects of EGFR and ErbB2, suggests that co-targeting the catalytic domains of EGFR and HER-2 with a dual EGFR/HER-2 inhibitor may yield superior therapeutic outcomes compared with monotherapy [27–30].

In a recent publication [31], various benzimidazole-based compounds have demonstrated significant antiproliferative effects. For instance, compound **I** (Figure 1) exhibited greater anticancer activity than the standard chemotherapeutic agent 5-fluorouracil (5-FU) against MCF-7 breast cancer cells, with IC_{50} values of 5 and 7 μM, respectively. Moreover, it showed notable EGFR inhibitory activity, achieving an IC_{50} of 0.08 μM, which is comparable to that of the clinically approved EGFR inhibitor gefitinib ($IC_{50} = 0.01$ μM) [32]. Compound **II** (Figure 1) demonstrated IC_{50} values of 5.67 and 1.87 μM against MDA-MB-231 and MCF-7 cells, respectively, indicating greater potency than the reference drug erlotinib ($IC_{50} = 7.46$ and 4.58 μM, respectively). Among the series of synthesized benzimidazole derivatives, compounds **III** and **IV** (Figure 1) emerged as the most potent, with IC_{50} values ranging from 0.95 to 2.10 μM across multiple cancer cell lines, including Panc-1, HT-29, A-549, and MCF-7 [33]. In this context, Jubie et al. synthesized three hydrazone derivatives incorporating the 1H-benzimidazole scaffold and evaluated their anticancer efficacy against HER-2 and MCF-7 breast cancer cell lines using the MTT assay [34]. Among these, compound **V** (Figure 1) demonstrated superior anticancer activity compared with lapatinib, a well-known HER-2 inhibitor. Molecular docking analyses further confirmed its strong binding affinity to HER-2, supporting its potential as a promising anti-breast cancer agent.

Additionally, El-Meguid et al. developed a novel series of 6-benzoyl-1*H*-benzimidazole derivatives and evaluated their cytotoxicity against HeLa cells, with doxorubicin serving as the reference drug [35]. These compounds exhibited inhibitory activity against several tyrosine kinases (TKs), including EGFR, HER-2, PDGFR-β, and VEGFR-2, while displaying negligible toxicity toward normal cells, highlighting their therapeutic potential. Notably, compounds **VI** and **VII** demonstrated the most potent cytotoxic effects against HeLa cells, with IC_{50} values of 1.62 ± 0.16 μM and 1.44 ± 0.06 μM, respectively.

1.1 | Rationale Design

A number of investigations have identified essential pharmacophoric characteristics frequently shared among EGFR-TKIs (TK inhibitor). These fundamental structural components can be categorized into four primary regions: (i) A planar heteroaromatic ring system fills the adenine-binding pocket of the ATP site and can make hydrogen bonds with essential amino acid residues, including Met793, Thr854, and Thr790. This core generally includes a minimum of one hydrogen bond acceptor, commonly a nitrogen atom or a carbonyl group, which mimics the interaction between ATP's purine ring and the kinase hinge region. (ii) A terminal hydrophobic head group located within hydrophobic region I, enhancing molecular affinity via van der Waals interactions. (iii) An imino linkage (NH–spacer) that promotes hydrogen bonding with amino acids in the linker region, hence augmenting binding selectivity. A stretch of spacer connecting the hydrophobic tail and the hinge-binding moiety.

These spacers demonstrate significant structural diversity among EGFR inhibitors, ranging from straightforward one-atom linkers, as shown in gefitinib, erlotinib, afatinib, and dacomitinib, to more intricate aryl-based linkers present in compounds such as lapatinib and olafertinib. The EGFR binding pocket exhibits significant tolerance for enhanced spacer complexity. (iv) A hydrophobic tail moiety, which occupies hydrophobic region II, significantly enhances the stability of the contact with the kinase domain. A hydrophobic tail, with binding properties that fluctuate based on the molecular architecture of the inhibitor. In inhibitors with shortened spacers (e.g., gefitinib), this tail fills a profound hydrophobic cavity proximal to the hinge area. In contrast, in drugs with

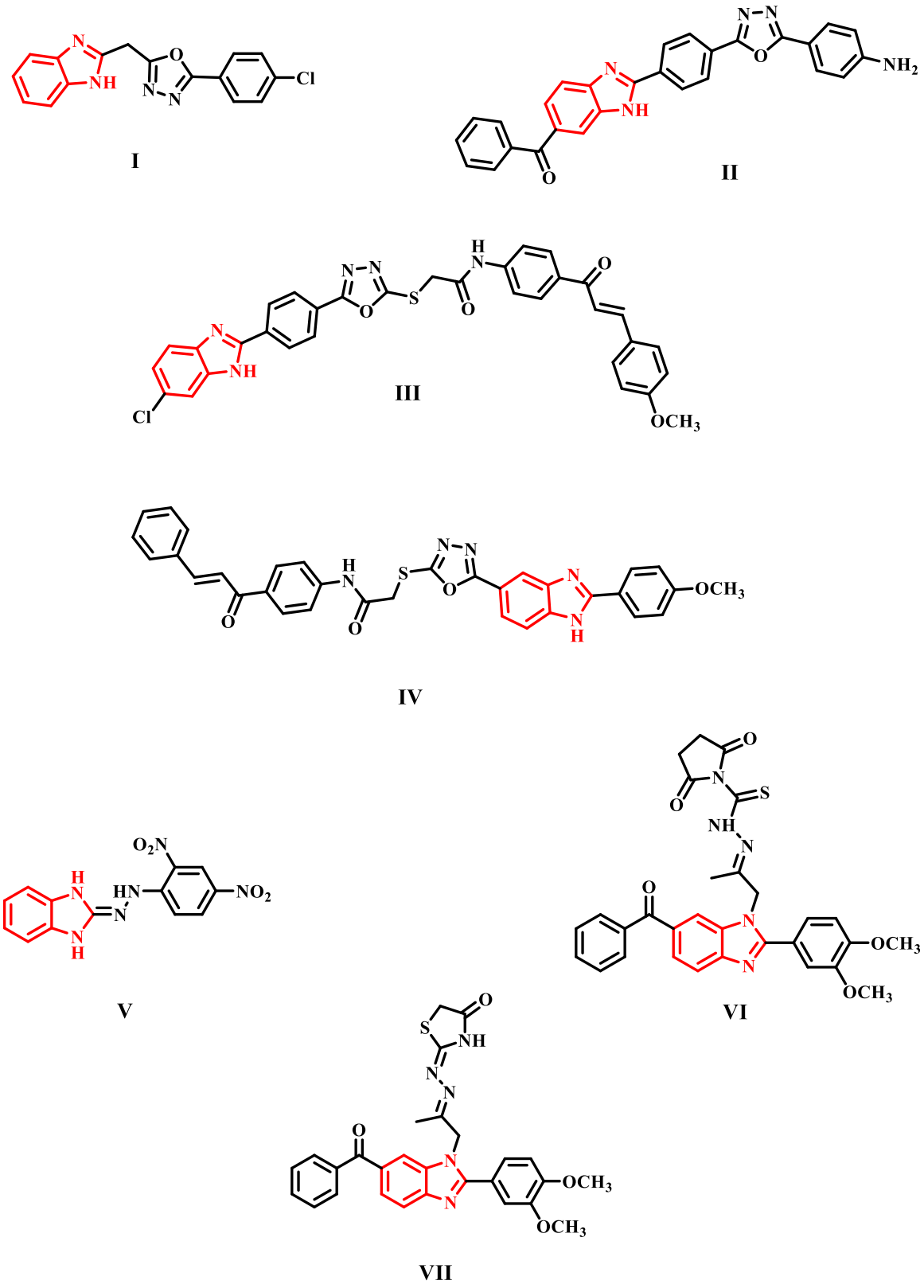

FIGURE 1 | Benzimidazole-based compounds (**I–VII**) as potent anticancer agents.

elongated spacers (e.g., lapatinib), the tail can access and interact with allosteric areas located farther from the hinge [36–43] (Figures 2–4).

In this study, we intend to design and synthesize a series of dual-targeted inhibitors for HER-2 and EGFR. Our molecular design strategy utilizes a substituted benzimidazole framework to occupy the ATP-binding sites of EGFR kinases. The spacer region incorporates an acyl hydrazone moiety introduced at the 5-position of the benzimidazole ring (**5a–g**). The spacer region can be rigidified by the triazole thione ring (**7a–b**), which acts as a flexible linker between the hinge-binding region and the DFG (Aspartate–Phenylalanine–Glycine) motif, along with an acid

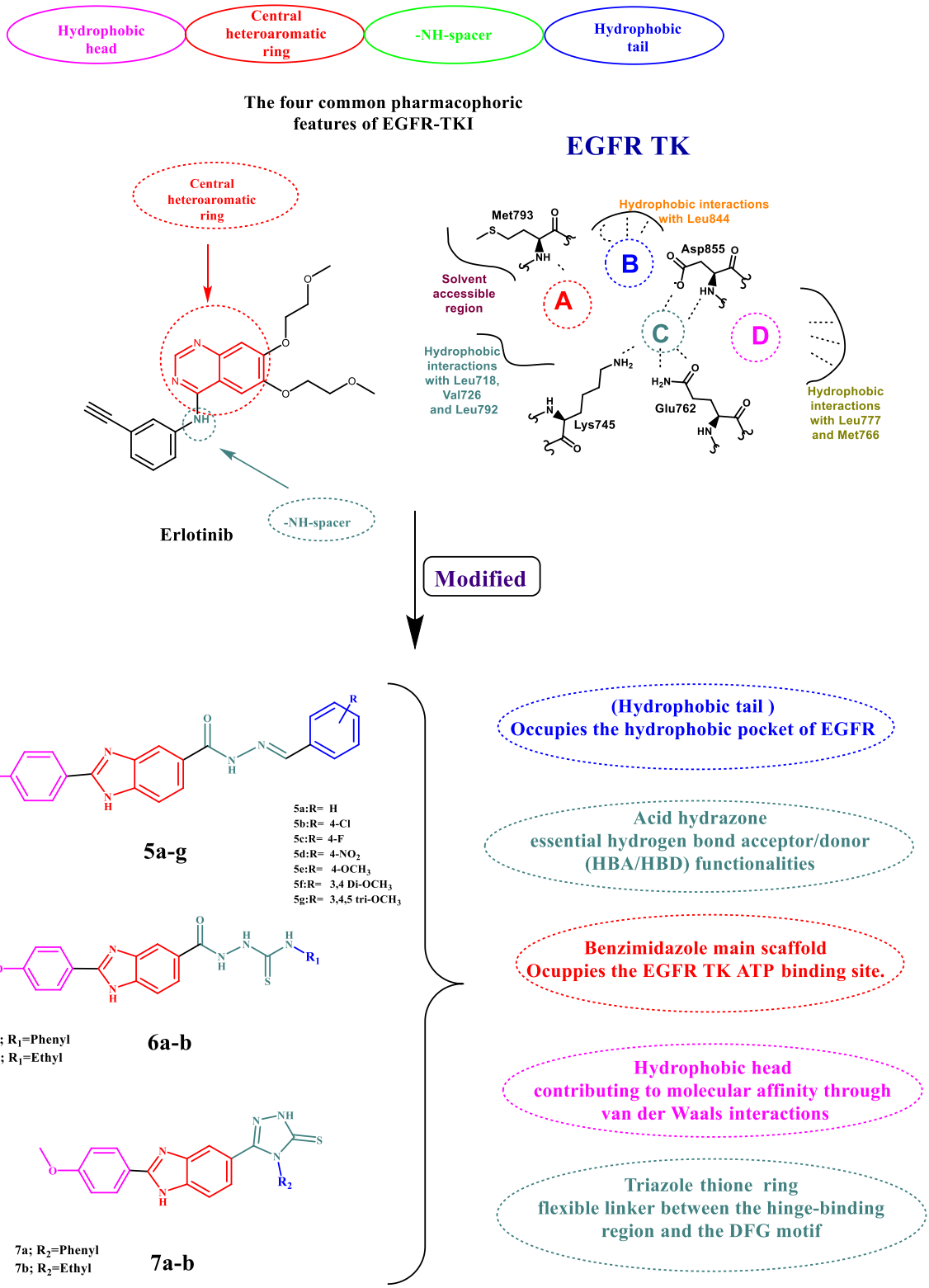

FIGURE 2 | Design and structures of the new benzimidazoles **5a–g**, **6a–b**, and **7a–b**.

hydrazone group that offers vital hydrogen bond acceptor/donor (HBA/HBD) functionalities, essential for replicating the EGFR pharmacophore. These spacer components have exhibited compatibility with EGFR, as evidenced by the aforementioned structural characteristics. The terminal hydrophobic segment is further modified with electron-withdrawing or electron-donating substituents, facilitating various hydrophobic interactions with the allosteric sites of both kinases (Figures 2–4).

2 | Results and Discussion

2.1 | Chemistry

Scheme 1 demonstrates the synthesis of compounds **5a–g, 6a–b**, and **7a–b**. Benzimidazole-5-carboxylic acid **3a** was synthesized in high yield by condensing 3,4-diaminobenzoic acid **1** with 4-methoxybenzaldehyde **2** in the presence of sodium metabisulphite and DMF [31]. Fischer esterification of carboxylic acid

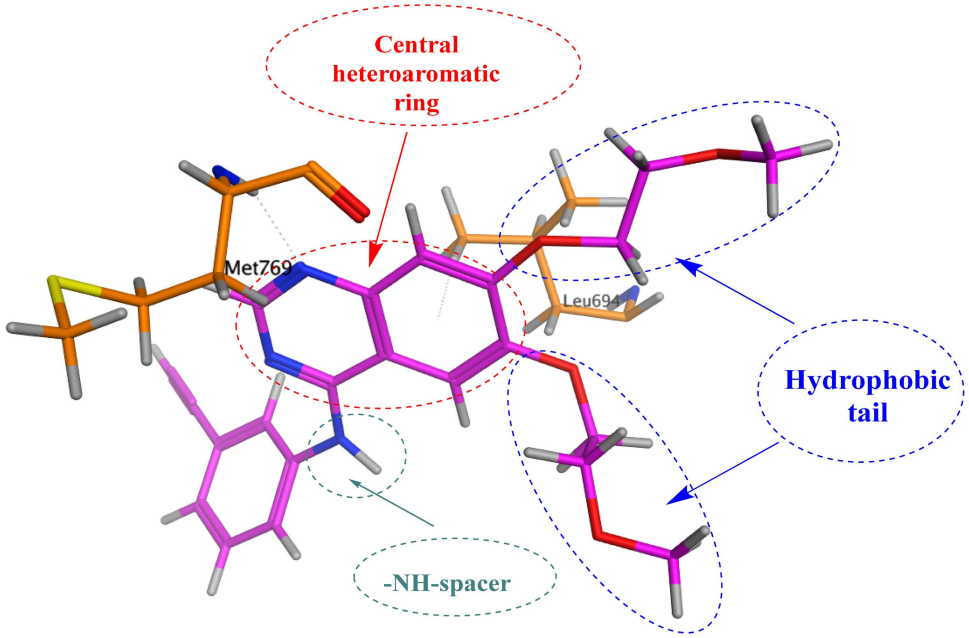

FIGURE 3 | Design and structure of 3D caption of Erlotinib within the EGFR binding pocket.

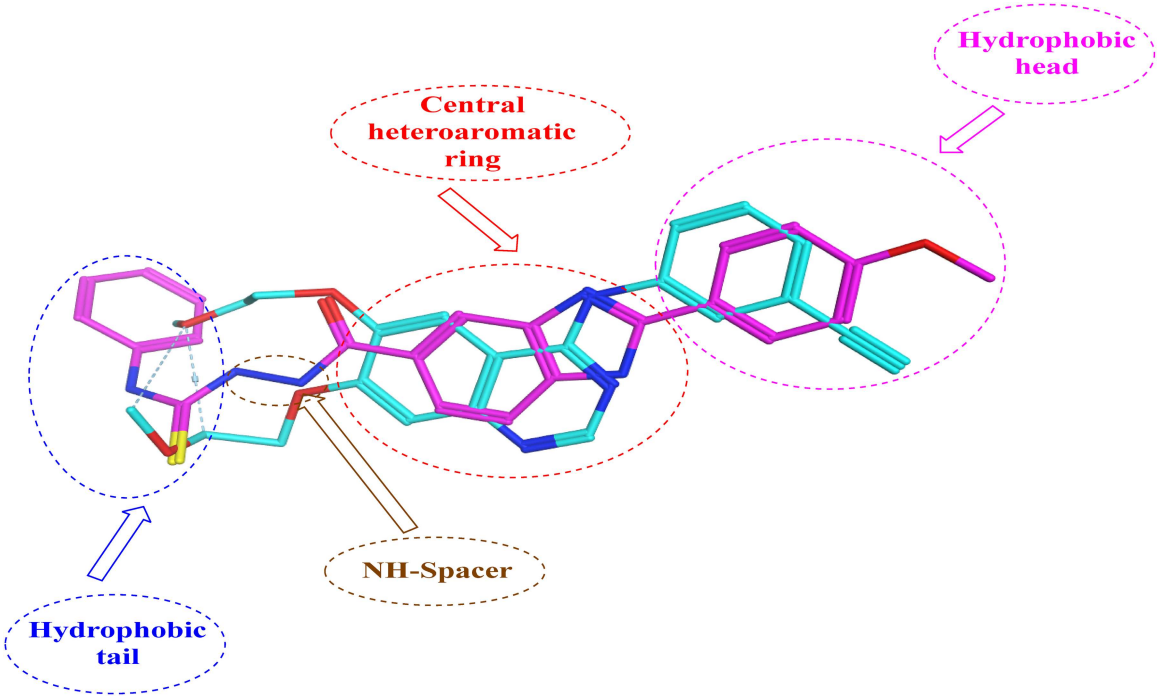

FIGURE 4 | 3D docking overlay of compound **6a** (pink color)with the reference anilinoquinazoline-based inhibitor erlotinib (Turquoise color).

3a was achieved to afford compound **3b** in 60% yield [44]. The hydrazide **4** was synthesized in 58% yield by heating the ester **3b** at reflux with 99% hydrazine monohydrate in ethanol [45]. The target compounds **5a–g** were synthesized in high yield by refluxing hydrazide **4** with substituted benzaldehyde in ethanol, and the structure of hydrazone derivatives **5a–g** was validated by different spectroscopic methods. The ^{1}H NMR spectra of compounds **5a–g** showed characteristic signals for the azomethine (CH═N) and hydrazone (NH) protons, while the ^{13}C NMR spectra confirmed the presence of the hydrazone (C═N) carbon, consistent with the proposed structures.

The thiosemicarbazide **6a–b** was prepared via heating at reflux of the hydrazide **4** with ethyl isothiocyanate in absolute ethanol. The ^{1}H NMR spectra of compounds **6a–b** showed characteristic signals corresponding to the thiosemicarbazide NH and ethyl protons, while the ^{13}C NMR spectra confirmed the presence of C═O, C═S, and ethyl carbon signals, consistent with the proposed structures.

The 1,2,4-triazole-3-thiones **7a–b** were synthesized through the cyclization of 1,4-disubstituted thiosemicarbazide **6a–b,** which involves the nucleophilic addition of terminal nitrogen atoms to the carbonyl group, followed by the elimination of water to

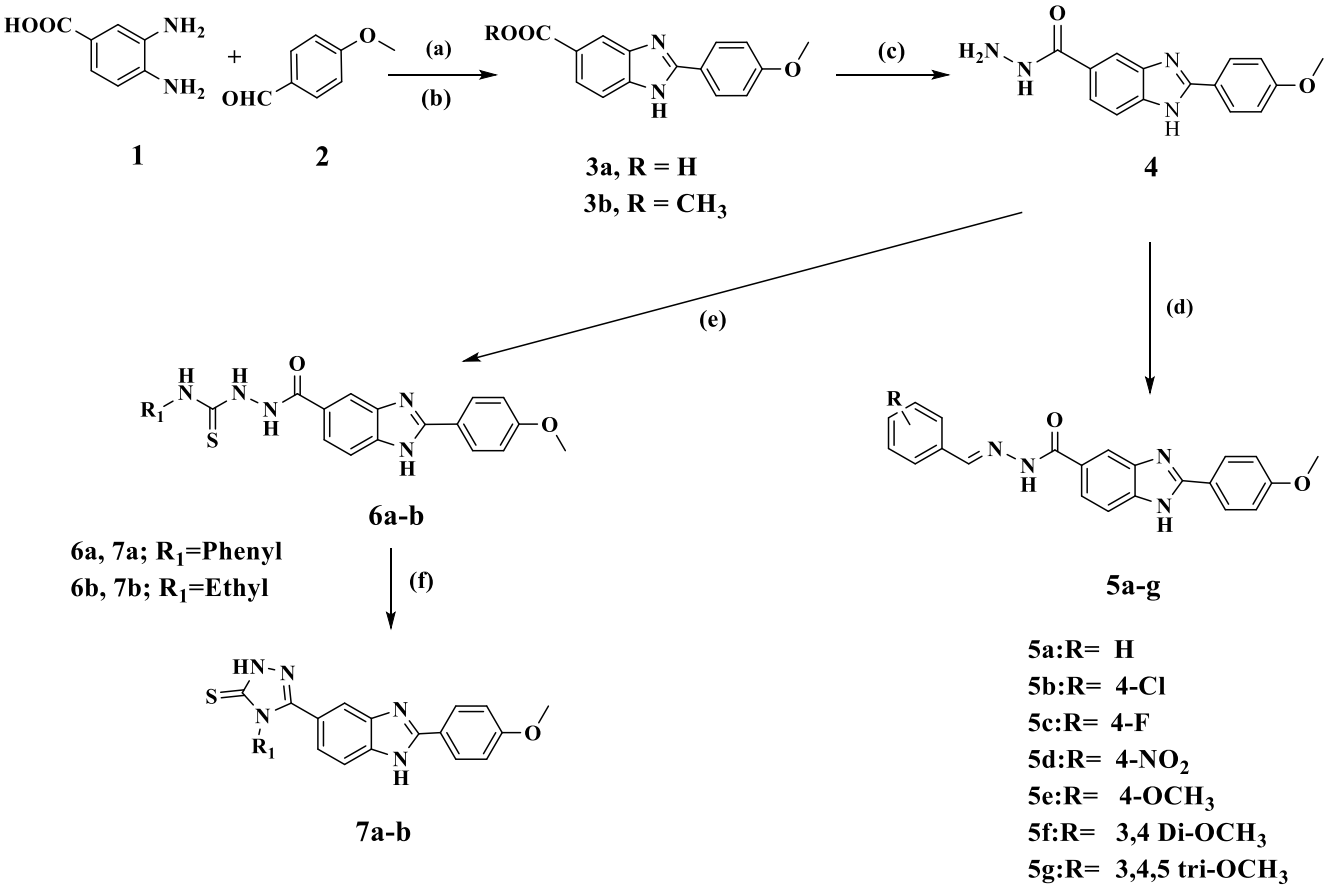

SCHEME 1 | Synthesis of target compounds **5a–g, 6a–b,** and **7a–b**. Reagent and reaction conditions: (a) DMF, $Na_2S_2O_8$; (b) Conc. H_2SO_4, methanol, reflux; (c) NH_2NH_2, H_2O; (d) aldehyde, CH_3COOH; (e) appropriate isothiocyanate, ethanol; reflux 6h; (f), NaOH.

yield the triazole products **7a–b**. The chemical structure of **7a–b** was determined by spectroscopic methods and elemental analysis. The ^1H NMR and ^{13}C NMR spectra of compounds **7a–b** confirmed the presence of triazole NH, ethyl, and C═S groups, in agreement with the proposed structures.

2.2 | Biology

2.2.1 | *Cell Viability Assay*

The impact of novel compounds **5a–g**, **6a–b**, and **7a–b** on the viability of a normal human cell line, specifically human mammary gland epithelial cells (MCF-10A), was assessed to ascertain the safety of the newly synthesized compounds. The MTT test was employed to assess the cell viability of the novel compounds after a 4-day incubation with MCF-10A cells [22, 46]. Table 1 indicates that none of the tested compounds exhibited cytotoxicity against normal cells; all compounds preserved cell viability above 89% at a concentration of 50 μM.

2.2.2 | *Antiproliferative Assay*

The in vitro antiproliferative effects of compounds **5a–g**, **6a–b**, and **7a-b** on two breast cancer cell lines (MCF-7 and MDA-MB231) were evaluated using the MTT test [17, 47]. The IC_{50} values for each compound were calculated, as shown in Table 2. Doxorubicin was employed as the reference drug.

TABLE 1 | Results of cell viability assay and IC_{50} values of compounds **5a–g, 6a–b,** and **7a–b**[a].

Compound	Cell viability %	Antiproliferative activity IC_{50} (μM)	
		MCF-7	MDA-MB231
5a	90	33 ± 2	40 ± 02
5b	92	6 ± 0.4	47 ± 02
5c	90	57 ± 3	245 ± 08
5d	93	72 ± 3	220 ± 06
5e	89	26 ± 2	235 ± 07
5f	90	8 ± 0.5	10 ± 0.5
5g	91	35 ± 2	230 ± 06
6a	94	5 ± 0.2	25 ± 01
6b	94	68 ± 3	250 ± 08
7a	90	15 ± 1	240 ± 07
7b	89	85 ± 4	20 ± 01
Doxorubicin	—	33 ± 3	3 ± 0.10

[a]The "cell viability %" column refers to MCF-10A cells, and that MTT assays were used to determine cytotoxicity.

An analysis of the results in Table 1 indicates that compounds **5a–g**, **6a–b**, and **7a–b** demonstrate greater efficacy against the MCF-7 breast cancer cell line compared with the MDA-MB231cell line. The IC_{50} values for compounds **5a–g**, **6a–b**, and

TABLE 2 | IC_{50} values of compounds **5b, 5f,** and **6a** against EGFR and HER-2.

Comp.	EGFR $IC_{50} \pm$ SEM (nM)	HER-2 $IC_{50} \pm$ SEM (nM)
5b	97 ± 5	74 ± 3
5f	125 ± 6	89 ± 5
6a	76 ± 3	60 ± 2
Erlotinib	80 ± 3	—
Lapatinib	—	26 ± 1

7a–b against the MCF-7 cancer cell line range from 5 to 85 μM, in contrast to the doxorubicin IC_{50} value of 33 μM. Compounds **5a–g**, **6a–b**, and **7a–b** demonstrated IC_{50} values between 10 and 250 μM against the MDA-MB-231 breast cancer cell line, in comparison to the standard doxorubicin, which had an IC_{50} value of 3 μM.

Regarding action against the MCF-7 breast cancer cell line, compounds **5b**, **5f**, and **6a** exhibited the highest potency, with IC_{50} values of 6, 8, and 5 μM, respectively, rendering them at least four times more effective than the reference Doxorubicin (IC_{50} value = 33 μM). Compound **6a** (R_1 = Phenyl, thiosemicarbazide) displayed the best potency among all the produced compounds against the breast cancer (MCF-7) cell line. The IC_{50} value was 5 μM, indicating a potency that is six times more than that of the reference Doxorubicin, which has an IC_{50} value of 33 μM. The substitution of the phenyl group at N1 in the thiosemicarbazide moiety with an ethyl group, as observed in compound **6b** (R_1 = ethyl, thiosemicarbazide), resulted in a significant decrease in antiproliferative activity. The IC_{50} value for component **6b** was 68 μM. The data indicate that the presence of a phenyl group is well-tolerated and promotes activity, but the ethyl group is not conducive to activity.

Compounds **5b** (R_1 = 4-Cl, Schiff base) and **5f** (R_1 = 3,4-di-OMe, Schiff base) exhibited the second and third-highest activity, with IC_{50} values of 6 and 8 μM, respectively. Compounds **5b** and **5f** demonstrated five- and fourfold better efficacy than doxorubicin against the MCF-7 breast cancer cell line. The substitution of the chlorine atom in the *para* position of the phenyl group of Schiff bases **5a–g** with a fluorine atom, as in compound **5c** (R_1 = 4-F, Schiff base), or with a nitro group, as in compound **5d** (R_1 = 4-NO2, Schiff base), resulted in an immense decrease in antiproliferative activity. The IC_{50} values were 57 μM for compound **5c** and 72 μM for compound **5d**. The data indicate that the substitution pattern at the *para* position of the phenyl group in Schiff bases **5a–g** substantially influences the antiproliferative action of these compounds. The presence of a fluorine atom or nitro group is not conducive to action. Conversely, the unsubstituted derivative, compound **5a** (R_1 = H, Schiff base), the 4-methoxy derivative, compound **5e** (R_1 = 4-OMe, Schiff base), and compound **5g** (R_1 = 3,4,5-tri-OMe, Schiff base) demonstrate significant antiproliferative activity with IC_{50} values of 33, 26, and 35 μM, being at least four times less potent than compound **5b**, yet still comparable to or even more potent than doxorubicin.

Ultimately, the 1,2,4-triazole derivative, compound **7a** (R_1 = Ph), had the fourth highest activity with an IC_{50} value of 15 μM, demonstrating a potency threefold inferior to that of the thiosemicarbazide derivative **6a**, although still exhibiting a potency twofold superior to the reference doxorubicin (IC_{50} = 33 μM). Once more, the ethyl-1,2,4-triazole derivative **7b** (R_1 = ethyl) demonstrated inferior activity compared with the phenyl-1,2,4-triazole derivative **7a**. Compound **7b** had an IC_{50} value of 85 μM, rendering **7b** the least efficient derivative among all newly synthesized compounds against the breast cancer cell line (MCF-7), highlighting the importance of the phenyl group for antiproliferative action.

2.2.3 | *EGFR Inhibitory Assay*

Compounds **5b**, **5f**, and **6a**, demonstrating the greatest efficacy as antiproliferative agents, were subsequently evaluated for their capacity to target the EGFR-TK [48, 49], a likely target for their effective antiproliferative action. The IC_{50} values for each compound were determined and compared to Erlotinib, which acted as a reference. Table 2 enumerates the IC_{50} values.

The outcomes of this in vitro assay are congruent with the findings of the antiproliferative assay. Compound **6a** (R_1 = Ph; thiosemicarbazide), the most potent antiproliferative agent, also exhibited the highest efficacy as an EGFR inhibitor, with an IC_{50} value of 76 nM. It exhibited comparable potency to the reference Erlotinib (IC_{50} value = 80 nM). Compounds **5b** and **5f** exhibited noteworthy EGFR inhibitory effects, with IC_{50} values of 97 nM and 125 nM, respectively. This indicates they were 1.2- and 1.6-fold less effective as EGFR inhibitors compared with Erlotinib. The data suggest that compound **6a** is an effective antiproliferative agent that may act as an EGFR inhibitor.

2.2.4 | *HER-2 Inhibitory Activity*

Compounds **5b**, **5f**, and **6a** were subsequently evaluated for their inhibitory effects on HER-2 TK [27, 50], utilizing Lapatinib as a reference compound. Results are presented in Table 2. Compound **6a** emerged as the most effective HER-2 inhibitor, with an IC_{50} value of 60 nM, whereas the reference Lapatinib demonstrated an IC_{50} value of 26 nM. The in vitro assay data indicated that compound **6a** is an effective antiproliferative drug suitable for use as an anti-breast cancer treatment, exhibiting dual targeting capabilities against EGFR and HER-2.

2.3 | Molecular Docking

Molecular docking was performed using AutoDock Vina within the PyRx platform. The docking search grid boxes were set based on the co-crystallized ligands to fully enclose them, with a total size of 25 $Å^3$ and coordinates $x = 22.013690$, $y = 0.252828$, $z = 52.794034$. Exhaustiveness was set to 24, generating 10 poses per docking experiment. Docking poses were visualized using PyMOL v3.1.0, and 2D captions were generated using BIOVIA Discovery Studio v25.1.0.24284. The protocol was validated by re-docking Erlotinib into the EGFR active site, with the top-scoring pose showing good alignment with the co-crystallized ligand (RMSD = 0.988 Å), Table 3 [52].

Compound **6a** showed a comparable interaction to the ATP-binding site of EGFR TK. It formed a strong interaction with Met769 key residue within the binding site, with overall binding affinity of −8.9 kcal/mol if compared to the positive control Erlotinib with a binding score of −8.3 kcal/mol. On the other

TABLE 3 | Molecular docking results for compounds **6a, 6b,** and Erlotinib during docking in the crystal structure of EGFR domain with 4-anilinoquinazoline inhibitor erlotinib (PDB ID: 1M17) active domain (Erlotinib as reference drug) [51]; including binding affinities (kcal/mol), distance (Å) from main residue contacts and type of the interaction.

EGFR Tyrosine Kinase (PDB ID: 1M17)				
Compound	**Affinity (kcal/mol)**	**Distance (in Å) from main residue**		**Type of interaction**
6a	−8.9	2.69	Met769	H-bond donor
		3.71	Leu694	Hydrophobic
		3.61	Asp831	H-bond acceptor
		3.22	Arg817	H-bond acceptor
		4.01	Lys704	Hydrophobic
		4.37	Leu768	Hydrophobic
6b	−7.4	4.07	Asp831	H-bond acceptor
		4.61	Leu820	Hydrophobic
		4.22	Leu694	Hydrophobic
		2.98	Phe699	Hydrophobic
Erlotinib	−8.3	1.60	Met769	H-bond acceptor
		3.55	Leu694	Hydrophobic
		3.21	Leu764	Hydrophobic
		3.80	Lys721	Hydrophobic

hand, compound **6b**, the ethyl derivative, showed a binding affinity of −7.4 kcal/mol with no interaction to the key amino acid Met769 that could explain the superior activity of the phenyl derivative compound **6a** over the ethyl derivative compound **6b** as an EGFR TK inhibitor (Figures 5–8).

2.4 | ADMET Studies

Compound **6a** and the orally active positive control drug erlotinib were converted into Simplified Molecular Input Line Entry System (SMILES) format. The pharmacokinetic prediction capabilities of online pkCSM (https://biosig.lab.uq.edu.au/pkcsm/) were employed to ascertain the pharmacokinetic parameters of the drugs analyzed [53]. ADMET prediction results indicated low aqueous solubility for both compound **6a** and the reference drug erlotinib, with predicted clogS values of (−2.892 and −5.144, respectively). Additionally, PKCSM software was utilized to predict certain ADMET parameters that may affect the pharmacokinetics of the synthesized medicines, Table 4.

This entailed quantifying the blood–brain barrier (BBB) partition coefficient, an essential parameter for pharmaceuticals targeting the brain with therapeutic effectiveness (a compound with clog BB > 0.3 can penetrate the BBB) [54]. Compound **6a** exhibits insufficient probability for permeating the BBB. Pharmaceuticals having a low probability of penetrating the BBB demonstrate little deleterious effect on the central nervous system. The Caco2 permeability coefficient, which measures the translocation of substances across a monolayer of human colon adenocarcinoma cells with tight junctions, was another variable component, serving as a model for paracellular transport (high Caco2 permeability > 0.90) [55]. Compound **6a** demonstrated increased permeability in Caco-2 cells.

Furthermore, the inhibition of cytochrome P450 3A4 (CYP450 3A4) has been effective in evaluating drug–drug interactions. Compound **6a** demonstrates a potential drug–drug interaction and shows a markedly enhanced projected total clearance value. It should be noted that all ADMET-related data, including drug–drug interaction potential and clearance values, are predictive and were obtained using the pkCSM computational tool. No experimental (in vitro or in vivo) measurements were conducted; therefore, these results represent in silico estimations only. The software incorporates a mechanism for predicting the toxicity profile of chemicals, including potential hepatotoxicity consequences.

Compound **6a** had a satisfactory safety profile for cardiotoxicity, particularly concerning the human ether-a-go-go-associated gene I, which displayed an acceptable safety margin. Moreover, hepatotoxicity is considered a critical factor, with the analyzed medications exhibiting adherence to an acceptable range. Unlike erlotinib, which may cause hepatotoxicity with extended use.

In-silico ADME/Tox predictions suggest that compound **6a** is anticipated to exhibit superior pharmacokinetic properties and an advantageous safety profile. This suggests its potential as a feasible option for oral treatment of cancer.

3 | Conclusion

The present study successfully identified a new class of benzimidazole-based derivatives **(5a–g)**, **(6a–b)**, and **(7a–b)** with promising dual inhibitory activity against EGFR and HER-2, highlighting their potential as anticancer agents. Among the synthesized compounds, **5b, 5f,** and particularly **6a** demonstrated superior antiproliferative effects, significantly outperforming the reference drug Doxorubicin in vitro. The remarkable efficacy of

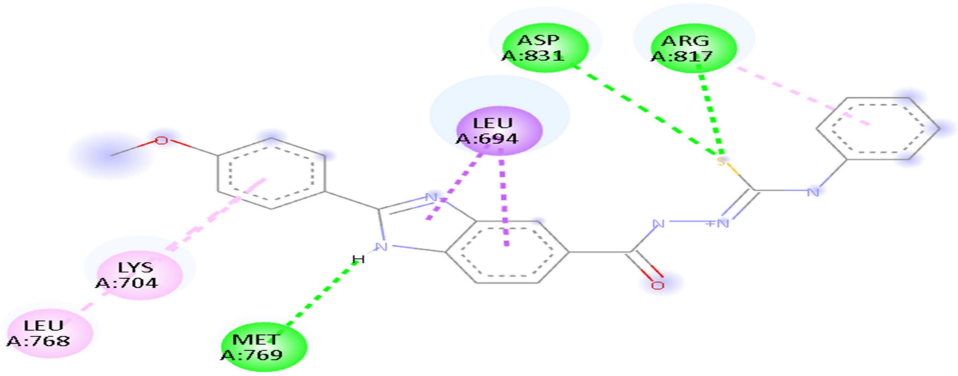

FIGURE 5 | 2D caption of compound **6a** showed the binding modes to the active site of EGFR TK active site.

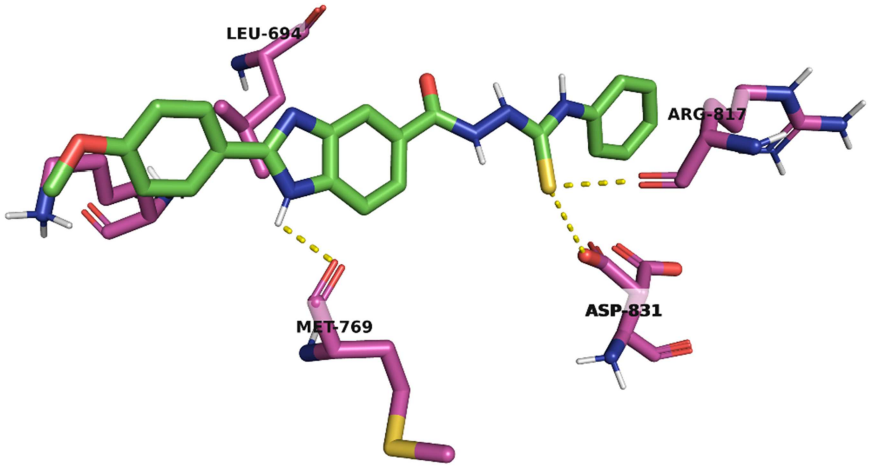

FIGURE 6 | 3D caption of compound **6a** showed the binding modes to the active site of EGFR TK active site.

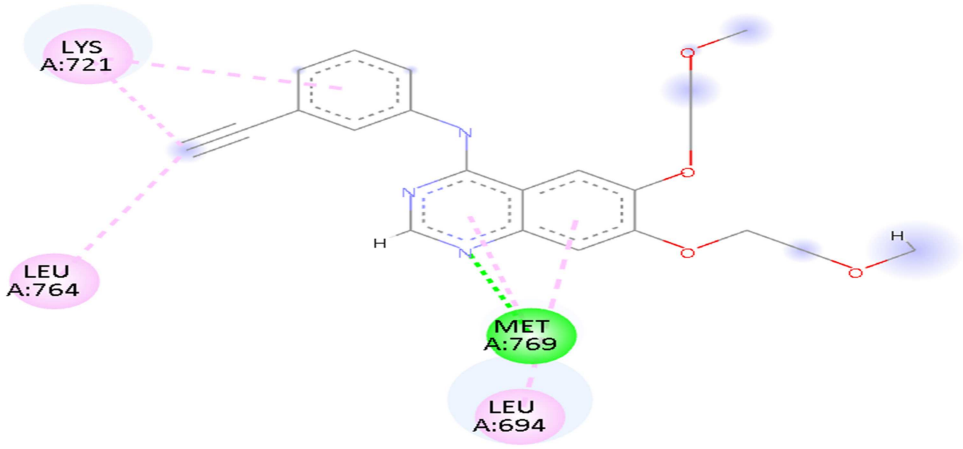

FIGURE 7 | 2D caption of **erlotinib** showed the binding modes to the active site of EGFR TK active site.

compound **6a** against MCF-7 cells, alongside its favorable binding interactions observed in molecular docking studies, underscores its potential as a lead candidate for further development. Moreover, the comparative lack of activity in compound **7b** reinforces the critical role of structural features, such as the phenyl group, in modulating biological activity. These findings warrant further pharmacological and mechanistic studies to optimize and validate the therapeutic potential of these derivatives in cancer treatment.

4 | Experimental

4.1 | Chemistry

4.1.1 | *General Details*

See Appendix A (Supplementary File).

The synthesized compounds were characterized using NMR spectroscopy and elemental analyses. The purity of the compounds was confirmed by UPLC. All corresponding

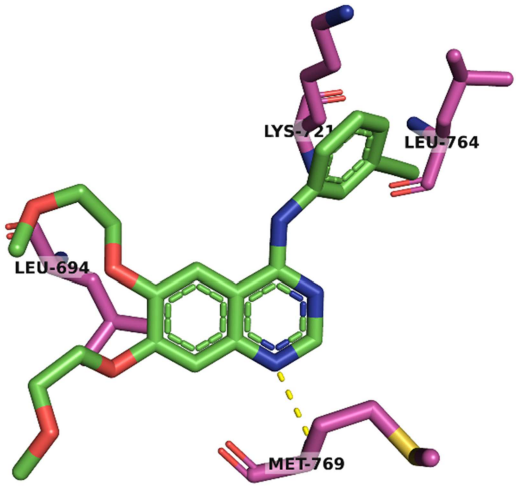

FIGURE 8 | 3D caption of **erlotinib** showed the binding modes to the active site of EGFR TK active site.

spectra and chromatograms are provided in the Supporting Information.

The key intermediates **3a, 3b,** and **4** were prepared according to previously reported procedures [30–32].

4.1.2 | General Procedure for Synthesis N′-Benzylidene-2-(4-methoxyphenyl)-1H-benzoimidazole-5-carbohydrazide (5a–g)

Equimolar ratios of hydrazide **4** (2 mmol, 0.50 g) and the corresponding benzaldehyde (2 mmol) in absolute ethanol (25 mL) were subjected to reflux for 6 h using glacial acetic acid as a catalyst. The resultant precipitate was filtered and recrystallized from ethanol, affording compounds **5a–g** in good yields.

4.1.2.1 | N′-Benzylidene-2-(4-methoxyphenyl)-1H-benzoimidazole-5-carbohydrazide (5a)

Grey powder, 80% yield, m. p: 206°C–208°C; ^{1}H NMR (DMSO-d_6, 400 MHz, δ ppm): 3.86 (s, 3H, OCH_3), 7.15 (d, 3H, $J = 8.00$ Hz, Ar-H), 7.47 (d, 4H, $J = 8.00$ Hz, Ar-H), 7.76 (d, 2H, $J = 8.00$ Hz, Ar-H), 7.82 (d, 1H, $J = 8.00$ Hz, Ar-H), 8.18 (d, 2H, $J = 12.00$ Hz, Ar-H), 8.52 (s, 1H, CH═NH), 11.89 (s, 1H, NH, hydrazone), 13.06 (s, 1H, NH benzimidazole); ^{13}C NMR (DMSO-d_6, 100 MHz, δ ppm): 55.86 (OCH_3), 114.71(Ar-C), 114.96 (Ar-CH), 115.05(Ar-CH), 122.59(Ar-CH benzimidazole), 127.44(Ar-CH benzimidazole), 127.46(Ar-CH benzimidazole), 127.55 (Ar-C C═O), 127.62 (Ar-CH C═N), 128.66 (Ar-CH C═N), 128.83 (Ar-CH C═N), 128.94 (Ar-CH), 129.30 (Ar-CH), 129.32 (Ar-CH C═N), 129.32 (Ar-C C═N), 129.33 (Ar-CH C═N), 130.43 (Ar-C benzimidazole), 130.47(Ar-C benzimidazole), 134.95 (C═N hydrazone), 147.81 (C═N benzimidazole), 161.50 (Ar-C C–O), 164.20 (C═O); Elemental analysis calculated for $C_{22}H_{18}N_4O_2$ (M. Wt.: 370.41): C, 71.34; H, 4.90; N, 15.13; O, 8.64; Found C, 71.21; H, 5.12; N, 15.30.

4.1.2.2 | (4-Chlorobenzylidene)-2-(4-methoxyphenyl)-1H-benzoimidazole-5-carbohydrazide (5b)

Grey powder, 85% yield, m.p: 238°C–240°C; ^{1}H NMR (DMSO-d_6, 400 MHz, δ ppm): 3.86 (s, 3H, OCH_3), 7.15 (d, 2H, $J = 8.00$ Hz, Ar-H), 7.53 (d, 2H, $J = 8.00$ Hz, Ar-H), 7.79 (m, 3H, Ar-H), 8.20 (m, 4H, Ar-H), 8.51 (s, 1H, CH═NH), 11.95 (s, 1H, NH, hydrazone), 13.07 (s, 1H, NH benzimidazole); ^{13}C NMR (DMSO-d_6, 100 MHz, δ ppm): 55.84 (OCH_3),111.42 (Ar-C), 114.32 (Ar-CH), 114.94 (Ar-CH), 115.28 (Ar-CH benzimidazole), 122.65 (Ar-CH benzimidazole), 128.79 (Ar-CH benzimidazole), 128.86 (Ar-C C═O), 128.89(Ar-CH C═N), 129.06 (Ar-CH C═N), 129.09 (Ar-CH C═N), 129.12 (Ar-CH), 129.36 (Ar-CH), 129.39 (Ar-CH C═N), 129.40 (Ar-C C═N), 129.41 (Ar-C C═N), 133.95 (Ar-C benzimidazole), 134.83 (Ar-C benzimidazole), 146.32 (C═N hydrazone), 153.71 (C═N benzimidazole), 161.46 (Ar-C C–O), 164.24 (C═O); Elemental analysis calculated for $C_{22}H_{17}ClN_4O_2$ (M. Wt.: 404.85): C, 65.27; H, 4.23; Cl, 8.76; N, 13.84; O, 7.90; Found C, 65.50; H, 4.37; N, 14.05.

4.1.2.3 | N′-(4-Fluorobenzylidene)-2-(4-methoxyphenyl)-1H-benzoimidazole-5-carbohydrazide (5c)

Grey powder, 78% yield, m. p: 234°C–236°C; ^{1}H NMR (DMSO-d_6, 400 MHz, δ ppm): 3.86 (s, 3H, OCH_3), 7.15 (d, 2H, $J = 8.00$ Hz, Ar-H), 7.30 (t, 2H, $J = 8.00$ Hz, Ar-H), 7.61 (d, 1H, $J = 8.00$ Hz, Ar-H), 7.82 (d, 4H, $J = 8.00$ Hz, Ar-H), 8.18 (d, 3H, $J = 12.00$ Hz, Ar-H), 8.52 (s, 1H, CH═NH), 11.90 (s, 1H, NH, hydrazone); ^{13}C NMR (DMSO-d_6, 100 MHz, δ ppm): 55.85 (OCH_3),114.92 (Ar-C), 114.95 (Ar-CH), 114.97 (Ar-CH), 116.24 (Ar-CH benzimidazole), 116.25 (Ar-CH benzimidazole), 116.45 (Ar-CH benzimidazole), 116.46 (Ar-C C═O), 122.60 (Ar-CH C═N), 127.40 (Ar-CH C═N), 128.83 (Ar-CH C═N), 128.84 (Ar-CH), 129.61 (Ar-CH), 129.61 (Ar-CH C═N), 129.67 (Ar-C C═N), 129.69 (Ar-C benzimidazole), 131.58 (Ar-C benzimidazole), 146.62 (C═N hydrazone), 153.98 (C═N benzimidazole), 161.49(Ar-C C–O), 162.29 (Ar-C F), 164.22 (C═O); Elemental analysis calculated for $C_{22}H_{17}FN_4O_2$ (M. Wt.: 388.39): C, 68.03; H, 4.41; F, 4.89; N, 14.43; O, 8.24; Found C, 68.22; H, 4.59; N, 14.71.

4.1.2.4 | 2-(4-Methoxyphenyl)-N′-(4-Nitrobenzylidene)-1H-benzoimidazole-5-carbohydrazide (5 d)

Yellow powder, 75% yield, m. p: 219°C–221°C; ^{1}H NMR (DMSO-d_6, 400 MHz, δ ppm): 3.86 (s, 3H, OCH_3), 7.14 (d, 2H, $J = 8.00$ Hz, Ar-H), 7.67 (d, 1H $J = 8.00$ Hz, Ar-H), 7.83 (m, 1H, Ar-H), 7.99 (d, 2H, $J = 8.00$ Hz, Ar-H), 8.15 (m, 2H, Ar-H), 8.30 (d, 3H, $J = 8.00$ Hz, Ar-H), 8.59 (s, 1H, CH═NH), 12.19 (s, 1H, NH, hydrazone), 13.07 (s, 1H, NH benzimidazole,); ^{13}C NMR (DMSO-d_6, 100 MHz, δ ppm): 55.84 (OCH_3), 111.46 (Ar-C), 114.90 (Ar-CH), 114.93 (Ar-CH), 114.94 (Ar-CH benzimidazole), 118.77 (Ar-CH benzimidazole), 122.60 (Ar-CH benzimidazole), 124.50 (Ar-C C═O), 124.5283 (Ar-CH C═N), 126.88 83 (Ar-CH C═N), 128.3083 (Ar-CH C═N), 128.33 (Ar-CH), 128.36 (Ar-CH), 128.78 (Ar-CH C═N), 128.92 (Ar-C C═N), 141.33 (Ar-C benzimidazole), 143.88 (Ar-C benzimidazole), 145.04 (C═N hydrazone), 148.19 (Ar-C NO_2), 153.75 (C═N benzimidazole), 161.46 (Ar-C C–O), 164.45 (C═O); Elemental analysis calculated for $C_{22}H_{17}N_5O_4$ (M. Wt.: 415.40): C, 63.61; H, 4.12; N, 16.86; O, 15.41; Found C, 63.87; H, 4.30; N, 17.04.

4.1.2.5 | N′-(4-Methoxybenzylidene)-2-(4-methoxyphenyl)-1H-benzoimidazole-5-carbohydrazide (5e)

Grey powder, 82% yield, m. p: 247°C–249°C; ^{1}H NMR (DMSO-d_6, 400 MHz, δ ppm): 3.82 (s, 3H, OCH_3), 3.86 (s, 3H, OCH_3), 7.04 (d, 2H, $J = 8.00$ Hz, Ar-H), 7.15 (d, 2H $J = 8.00$ Hz, Ar-H), 7.69

TABLE 4 | ADMET studies for compound 6a.

Parameter	Model name	Unit	6a	Reference
Molecular properties	Molecular Weight	amu	417.494	< 500
	LogP	Numeric	3.8699	> 5
	Donors	Numeric	4	> 5
	Acceptors	Numeric	4	> 10
	Rotatable bonds	Numeric	4	> 5
Absorption	Water solubility	Numeric (log mol L^{-1})	−2.892	Solubility decreased by increasing log S
	Intestinal absorption (human)	Numeric (% absorbed)	82.882	Poorly absorbed > 30%
	Caco2 permeability	Numeric (log Papp in 10^{-6} cm s^{-1})	1.051	Low permeability > 0.90
	Skin Permeability	Numeric (log Kp)	−2.735	Logkp > −2.5
	P-glycoprotein I inhibitor	Categorical (Yes/No)	No	—
	P-glycoprotein II inhibitor	Categorical (Yes/No)	Yes	—
	P-glycoprotein substrate	Categorical (Yes/No)	Yes	—
Distribution	Fraction unbound (human)	Numeric (Fu)	0.281	High > 0.45
	VDss (human)	Numeric (log L kg^{-1})	0.082	Log VDss is considered Low < −0.15. Log VDss is considered high > 0.45
	CNS permeability	Numeric (log PS)	−2.254	– Log PS < −3 unable to penetrate CNS – Log PS > −2 penetrate CNS
	BBB permeability	Numeric (log BB)	−0.813	– Log BB < −1 poorly distributed to the brain – Log BB > 0.3 cross the BBB
Metabolism	CYP1A2 inhibitor	Categorical (yes/no)	Yes	This can be positively correlated to the lipophilicity of the compound to metabolism related toxicity
	CYP2C19 inhibitor	Categorical (yes/no)	Yes	
	CYP2C9 inhibitor	Categorical (yes/no)	Yes	
	CYP2D6 inhibitor	Categorical (yes/no)	No	
	CYP3A4 inhibitor	Categorical (yes/no)	Yes	
	CYP2D6 substrate	Categorical (yes/no)	Yes	
	CYP3A4 substrate	Categorical (yes/no)	Yes	
Excretion	Renal OCT2 substrate	Categorical (yes/no)	Yes	—
	Total clearance	Numeric (log ml min^{-1} kg^{-1})	0.653	—
Toxicity	Hepatotoxicity	Categorical (yes/no)	Yes	
	Skin Sensitization	Categorical (yes/no)	No	

(Continues)

TABLE 4 | (Continued)

Parameter	Model name	Unit	6a	Reference
	hERG I inhibitor	Categorical (yes/no)	No	
	hERG II inhibitor	Categorical (yes/no)	Yes	
	AMES toxicity	Categorical (yes/no)	Yes	
	Oral Rat acute toxicity (LD50)	Numeric (mol kg^{-1})	2.49	
	Max. tolerated dose (human)	Numeric (log mg kg^{-1} per day)	0.342	Low ≤ 0.477 High > 0.477
	Oral Rat chronic toxicity (LOAEL)	Numeric (log mg kg^{-1}_bw per day)	3.391	
	Minnow toxicity	Numeric (log mM)	1.073	Highly acute toxic < −0.3 Not highly acute toxic > −0.3
	T. Pyriformis toxicity	Numeric (log ug L^{-1})	0.285	Not toxic < −0.5 Toxic > −0.5

(m, 4H, Ar-H), 7.81 (d, 1H, $J = 8.00$ Hz, Ar-H), 8.17 (d, 3H, $J = 8.00$ Hz, Ar-H), 8.46 (s, 1H, C**H**=NH), 11.75 (s, 1H, N**H**); ^{13}C NMR (DMSO-d_6, 100 MHz, δ ppm): 55.75 (O**C**H$_3$), 55.86 (O**C**H$_3$), 114.78(Ar-**C**),114.80(Ar-**C**H), 114.82(Ar-**C**H), 114.83(Ar-**C**H benzimidazole), 114.92 (Ar-**C**H benzimidazole), 114.95 (Ar-**C**H benzimidazole), 114.97(Ar-**C** C=O), 122.61(Ar-**C**H C=N), 122.62(Ar-**C**H C=N), 127.53(Ar-**C**H C=N), 127.59(Ar-**C**H), 128.79(Ar-**C**H), 128.82 (Ar-**C**H C=N), 128.85 (Ar-**C** C=N), 129.07(Ar-**C** benzimidazole), 129.12(Ar-**C** benzimidazole), 129.13(**C**=N hydrazone), 147.68(**C**=N benzimidazole), 161.22(Ar-**C** C–O), 161.47(Ar-**C** C–O), 164.04 (**C**=O); Elemental analysis calculated for $C_{23}H_{20}N_4O_3$ (M. Wt.: 400.43): C, 68.99; H, 5.03; N, 13.99; O, 11.99; Found C, 69.12; H, 5.15; N, 14.23.

4.1.2.6 | N′*-(3,4-Dimethoxybenzylidene)-2-(4-methoxyphenyl)-1*H*-benzoimidazole-5-carbohydrazide (5f)*

Grey powder, 78% yield, m. p: 226°C–228°C; ^{1}H NMR (DMSO-d_6, 400 MHz, δ ppm): 3.82 (s, 6H, OCH$_3$), 3.86 (s, 3H, OCH$_3$), 7.04 (d, 1H, $J = 8.00$ Hz, Ar-H), 7.15 (d, 2H $J = 8.00$ Hz, Ar-H), 7.23 (d, 1H, $J = 8.00$ Hz, Ar-H), 7.39 (s, 1H, Ar-H), 7.72 (m, 2H, Ar-H), 8.18 (m, 3H, Ar-H), 8.45 (s, 1H, C**H**=NH), 11.78 (s, 1H, N**H**, hydrazone), 13.06 (s, 1H, N**H** benzimidazole); ^{13}C NMR (DMSO-d_6, 100 MHz, δ ppm):55.83 (OCH$_3$), 55.85 (OCH$_3$), 56.03(OCH$_3$), 108.76(Ar-**C**), 111.38 (Ar-**C**H), 111.98 (Ar-**C**H), 114.95 (Ar-**C**H benzimidazole), 114.97 (Ar-**C**H benzimidazole), 118.50 (Ar-**C**H benzimidazole), 122.27(Ar-**C** C=O), 122.31(Ar-**C**H C=N), 122.69(Ar-**C**H C=N), 127.73 (Ar-**C**H C=N), 128.77 (Ar-**C**H), 128.81 (Ar-**C**H), 128.86 (Ar-**C** C=N), 135.16 (Ar-**C** benzimidazole), 137.96 (Ar-**C** benzimidazole), 147.94 (**C**=N hydrazone), 148.05 (Ar-**C** C-O), 149.57 (Ar-**C** C-O), 151.14 (**C**=N benzimidazole), 161.45(Ar-**C** C–O), 164.10 (**C**=O); Elemental analysis calculated for $C_{24}H_{22}N_4O_4$ (M. Wt.: 430.46): C, 66.97; H, 5.15; N, 13.02; O, 14.87; Found C, 67.08; H, 5.29; N, 13.27.

4.1.2.7 | *2-(4-Methoxyphenyl)-*N′*-(3,4,5-Trimethoxybenzylidene)-1*H*-benzoimidazole-5-carbohydrazide (5 g)*

Grey powder, 75% yield, m. p: 207°C–209°C; ^{1}H NMR (DMSO-d_6, 400 MHz, δ ppm): 3.73 (s, 3H, OCH$_3$), 3.86 (s, 9H, OCH$_3$), 7.06 (s, 2H, Ar-H), 7.15 (d, 2H $J = 8.00$ Hz, Ar-H), 7.81 (d, 2H, $J = 8.00$ Hz, Ar-H), 8.17 (d, 3H, $J = 8.00$ Hz, Ar-H), 8.45 (s, 1H, C**H**=NH), 11.88 (s, 1H, N**H**, hydrazone),13.07 (s, 1H, N**H** benzimidazole); ^{13}C NMR (DMSO-d_6, 100 MHz, δ ppm): 55.86 (O**C**H$_3$), 56.43 (O**C**H$_3$), 56.44 (O**C**H$_3$), 60.60 (O**C**H$_3$), 104.72 (Ar-**C**), 104.75 (Ar-**C**H), 104.77 (Ar-**C**H), 104.78 (Ar-**C**H benzimidazole), 114.93(Ar-**C**H benzimidazole), 114.95(Ar-**C**H benzimidazole), 114.97(Ar-**C** C=O), 114.98(Ar-**C**H C=N), 122.64(Ar-**C**H C=N), 128.77(Ar-**C**H C=N), 128.80(Ar-**C**H), 128.82 (Ar-**C**H), 128.86(Ar-**C**H benzimidazole),130.50 (Ar-**C** benzimidazole), 130.52 (Ar-**C** C–O), 139.62(**C**=N hydrazone), 147.76 (**C**=N benzimidazole), 153.6714(Ar-**C** C–O), 153.67(Ar-**C** C–O), 161.48(Ar-**C** C–O), 164.23(**C**=O); Elemental analysis calculated for $C_{25}H_{24}N_4O_5$ (M. Wt.: 460.48): C, 65.21; H, 5.25; N, 12.17; O, 17.37; Found C, 65.47; H, 5.33; N, 12.40.

4.1.3 | *General Procedure for the Synthesis of* N*-Ethyl-2-(2-(4-Methoxyphenyl)-1*H*-Benzoimidazole-5-Carbonyl) Hydrazine Carbothioamide Derivatives (6A-B)*

Equimolar amounts (2 mmol, 0.50 g) of compound **4** and the corresponding isothiocyanate (2 mmol) in absolute ethanol

(25 mL) were subjected to reflux for 6 h. The resultant solid was filtered and dried, then utilized in the subsequent step without additional purification to afford thiosemicarbazides **6a–b** in a good yield.

4.1.3.1 | *2-(4-Methoxyphenyl)-*N*-(2-Phenylhydrazine-1-Carbonothioyl)-1*H*-Benzimidazole-5-Carboxamide (6a)*

Beige powder, 63% yield, m. p: 209°C–211°C; ^{1}H NMR (DMSO-d_6, 400 MHz, δ ppm): 3.87 (s, 3H, OCH_3), 7.15 (d, 3H, $J = 8.00$ Hz, Ar-H), 7.35 (m, 2H, Ar-H), 7.50 (s, 2H, Ar-H), 7.85 (d, 1H, $J = 8.00$ Hz, Ar-H), 8.18 (d, 4H, $J = 8.00$ Hz, Ar-H), 9.72 (s, 1H, Ar-H), 9.86 (s, 1H, NH thiosemicarbazide), 10.53 (s,1H, NH thiosemicarbazide), 13.03(s,1H, NH benzimidazole); ^{13}C NMR (DMSO-d_6, 100 MHz, δ ppm): 55.87 (OCH_3), 114.91 (Ar-C), 114.94 (Ar-CH), 114.95 (Ar-CH), 115.04 (Ar-CH benzimidazole), 122.67 (Ar-CH benzimidazole), 122.69 (Ar-CH benzimidazole), 125.41 (Ar-C C═O), 125.49 (Ar-CH C═N), 126.45(Ar-C C═N), 126.58(Ar-CH C═N), 126.75 (Ar-CH C═N), 128.47 (Ar-CH C═N), 128.50(Ar-CH C═N), 128.50 (Ar-CH), 128.78 (Ar-CH), 128.79 (Ar-C benzimidazole), 128.82 (Ar-C benzimidazole), 128.86 (C═N benzimidazole), 139.80(Ar-C C–O), 161.46 (C═O), 167.09 (C═S); Elemental analysis calculated for $C_{22}H_{19}N_5O_2S$ (M. Wt.: 417.48): C, 63.29; H, 4.59; N, 16.78; O, 7.66; S, 7.68; Found C, 63.45; H, 4.67; N, 17.03; S, 7.75.

4.1.3.2 | N*-Ethyl-2-(2-(4-methoxyphenyl)-1*H*-benzoimidazole-5-carbonyl)hydrazine carbothioamide (6b)*

Grey powder, 63% yield, m. p: 239°C–241°C; ^{1}H NMR (DMSO-d_6, 400 MHz, δ ppm): 1.09 (t, 3H, $J = 8.00$ Hz, CH_3), 3.67 (q, 2H, $J = 8.00$ Hz, CH_2), 3.86 (s, 3H, OCH_3), 7.14 (d, 2H, $J = 8.00$ Hz, Ar-H), 7.73 (m, 2H, Ar-H), 8.19 (m, 4H, Ar-H), 9.24 (s, 1H, Ar-H), 10.31(s, 1H, NH thiosemicarbazide), 13.07(s.1H, NH benzimidazole); ^{13}C NMR (DMSO-d_6, 100 MHz, δ ppm): 14.97 (CH_3), 114.99 (CH_2), 55.86 (OCH_3), 114.93(Ar-C), 114.95(Ar-CH), 114.96(Ar-CH), 114.97 (Ar-CH benzimidazole), 122.51(Ar-CH benzimidazole), 122.56 (Ar-CH benzimidazole), 122.61 (Ar-C C═O), 126.57(Ar-CH), 128.78 (Ar-CH), 128.80 (Ar-C benzimidazole), 128.82 (Ar-C benzimidazole), 128.87 (C═N benzimidazole), 153.91 (Ar-C C–O), 161.47 (C═O), 167.15 (C═S); Elemental analysis calculated for $C_{18}H_{19}N_5O_2S$ (M. Wt.: 369.44): C, 58.52; H, 5.18; N, 18.96; O, 8.66; S, 8.68; Found C, 58.69; H, 5.37; N, 19.09; S, 8.62.

4.1.4 | *General Procedure for the Synthesis of 4-Ethyl-3-(2-(4-Methoxyphenyl)-1*H*-Benzoimidazol-5-Yl)-1*H*-1,2,4-Triazole-5(4*H*)-Thione (7a–b)*

Appropriate thiosemicarbazide **6a–b** (10 mmol) was dissolved in 2 N sodium hydroxide solution (20 mL) and subsequently subjected to reflux for 4 h. The solution was acidified with dilute HCl to a pH of 3; the resultant precipitate was filtered, washed with distilled water, dried, and subsequently recrystallized from ethanol to provide 1,2,4-triazoles **7a–b** in a good yield.

4.1.4.1 | *3-(2-(4-Methoxyphenyl)-1*H*-Benzoimidazol-5-Yl)-4-Phenyl-1*H*-1,2,4-Triazole-5(4*H*)-Thione (7a)*

Yellow powder, 65% yield, m. p: 237°C–239°C; ^{1}H NMR (DMSO-d_6, 400 MHz, δ ppm): 3.85 (s, 3H, OCH_3), 7.12 (m, 4H, Ar-H), 7.24 (d, 1H, $J = 8.00$ Hz, Ar-H), 7.40(d, 1H, $J = 8.00$ Hz, Ar-H), 7.44 (s, 1H, Ar-H), 7.52 (m, 2H, Ar-H), 7.64 (d, 1H, $J = 8.00$ Hz, Ar-H), 7.85 (d, 1H, $J = 8.00$ Hz, Ar-H), 8.09 (d, 1H, $J = 8.00$ Hz, Ar-H), 8.16 (d, 2H, $J = 8.00$ Hz, Ar-H); ^{13}C NMR (DMSO-d_6, 100 MHz, δ ppm): 55.87 (OCH_3), 114.93(Ar-CH), 114.97 (Ar-CH benzimidazole), 114.99 (Ar-CH benzimidazole), 115.01 (Ar-CH), 116.97 (Ar-CH), 122.11 (Ar-CH benzimidazole), 123.99 (Ar-CH benzimidazole), 124.93 (Ar-C N triazole), 128.84 (Ar-CH N triazole), 128.91 (Ar-CH N triazole), 128.94 (Ar-CH N triazole), 128.96 (Ar-CH N triazole), 129.25 (Ar-CH), 129.82 (Ar-CH), 129.83 (Ar-C N triazole), 151.84 (Ar-C benzimidazole), 153.56 (Ar-C benzimidazole), 154.05 (C═N triazole), 161.64(C═N benzimidazole), 168.33(Ar-C C–O), 168.92 (C═S); Elemental analysis calculated for $C_{22}H_{17}N_5OS$ (M. Wt.: 399.47): C, 66.15; H, 4.29; N, 17.53; O, 4.01; S, 8.03; Found C, 66.07; H, 4.40; N, 17.68; S, 8.20.

4.1.4.2 | *4-Ethyl-3-(2-(4-Methoxyphenyl)-1*H*-Benzoimidazol-5-Yl)-1*H*-1,2,4-Triazole-5(4*H*)-Thione (7B)*

Brown powder, 65% yield, m. p: 221°C–223°C; ^{1}H NMR (DMSO-*d*, 400 MHz, δ ppm): 1.18 (t, 3H, $J = 8.00$ Hz, CH_3), 3.81 (s, 3H, OCH_3), 4.09 (q, 2H, $J = 8.00$ Hz, CH_2), 7.09 (d, 2H, $J = 8.00$ Hz, Ar-H), 7.44 (d, 1H, $J = 8.00$ Hz, Ar-H), 7.62 (d, 1H, Ar-H), 7.73 (d, 1H, $J = 8.00$ Hz, Ar-H), 7.86 (d, 1H, $J = 8.00$ Hz, Ar-H), 8.19 (m, 3H, Ar-H); ^{13}C NMR (DMSO-d_6, 100 MHz, δ ppm): 13.91 (CH_3), 18.92 (CH_2), 55.77 (OCH_3), 114.85(Ar-C), 114.87(Ar-CH), 114.90(Ar-CH), 119.82(Ar-CH benzimidazole), 122.51(Ar-CH benzimidazole), 122.58(Ar-CH benzimidazole), 123.89(Ar-C N triazole), 126.11(Ar-CH), 128.85(Ar-CH), 128.88(Ar-C benzimidazole), 152.49(Ar-C benzimidazole), 154.01(C═N triazole), 161.42(C═N benzimidazole), 167.07 (Ar-C C–O), 168.98 (C═S); Elemental analysis calculated for $C_{18}H_{17}N_5OS$ (M. Wt.: 351.43): C, 61.52; H, 4.88; N, 19.93; O, 4.55; S, 9.12; Found C, 61.78; H, 5.03; N, 20.14; S, 9.31.

4.2 | Biology

4.2.1 | *Cell Viability Assay*

The impact of new compounds **5a–g**, **6a–b**, and **7a–b** on cell viability was evaluated utilizing the human mammary gland epithelial normal cell line (MCF-10A). The MTT assay was employed to assess the viability of **5a–g**, **6a–b**, and **7a–b** following 4 days of incubation with MCF-10A cells [43]. Refer to Supporting Information S1: Appendix A for additional information.

4.2.2 | *Antiproliferative Assay*

The MTT assay was employed to assess the antiproliferative effects of compounds **5a–g**, **6a–b**, and **7a–b** on two breast cancer cell lines (MCF-7 and MDA-MB231). Doxorubicin was employed as a reference [44]. The dose–response experiments established the IC_{50} values for the new compounds. The provided data were obtained from at least two different studies, each comprising three repeats per concentration. Supporting Information S1: Appendix A contains experimental specifics.

4.2.3 | *EGFR Inhibitory Assay*

Compounds **5c**, **5f**, and **6a** were evaluated for their capacity to inhibit EGFR via the EGFR-TK assay [45], with erlotinib

serving as the reference compound. Supporting Information S1: Appendix A has more information.

4.2.4 | *HER-2 Inhibitory Assay*

The compounds **5c**, **5f**, and **6a** were assessed for their ability to inhibit HER-2 using a kinase assay [47]. Lapatinib functioned as the reference compound. Consult Supporting Information S1: Appendix A.

4.3 | Molecular Docking

Molecular docking was conducted using AutoDock Vina within the PyRx platform.

The docking grid enclosed the co-crystallized ligands with coordinates $x = 22.01$, $y = 0.25$, $z = 52.79$ (25 Å^3 volume). Ten poses were generated per run with exhaustiveness set to 24.

Validation by re-docking Erlotinib into EGFR showed good alignment (RMSD = 0.988 Å).

Docking results were visualized using PyMOL and BIOVIA Discovery Studio [52].

4.3.1 | *Docking Procedures*

1. Ligand Structure Generation [56]

   Open Babel v.3. sed to convert the structures' SMILE codes to three-dimensional configurations that were subsequently subjected to a minimization of energy using the steepest descent technique with the same software. The minimization was performed by the force field MMFF94. Using AutoDock Tools v.4.2, all torsions of the selected structures were assigned, and their Gasteiger charges were provided for all studied atoms in structures.

2. Protein Structure Preparation [57]

   For docking screening, the crystal structure of Epidermal Growth Factor Receptor TK domain with 4-anilinoquinazoline inhibitor erlotinib (PDB ID: **1M17**) were used. PDBfixer was used to edit the downloaded structure, adding missing residues and atoms, and removing co-crystalized waters and agents. Through AutoDock Tools v.4.2, polar hydrogen and Gasteiger charges were subsequently made available for both proteins.

Funding

The authors received no specific funding for this work.

Conflicts of Interest

The authors declare no conflicts of interest.

Data Availability Statement

The data supporting this article have been included as part of the Supplementary Information.

References

1. R. C. Sobti, M. Thakur, and T. Kaur, *Cancer: Epidemiology, Racial, and Geographical Disparities, Molecular Biomarkers for Cancer Diagnosis and Therapy* (Springer, 2024), 31–52.

2. C. H. Barrios, "Global Challenges in Breast Cancer Detection and Treatment," *Breast* 62 (2022): S3–S6.

3. M. A. S. Abourehab, A. M. Alqahtani, B. G. M. Youssif, and A. M. Gouda, "Globally Approved EGFR Inhibitors: Insights Into Their Syntheses, Target Kinases, Biological Activities, Receptor Interactions, and Metabolism," *Molecules* 26, no. 21 (2021): 6677.

4. C. Tito, S. Masciarelli, G. Colotti, and F. Fazi, "EGF Receptor in Organ Development, Tissue Homeostasis and Regeneration," *Journal of Biomedical Science* 32, no. 1 (2025): 24.

5. L. Xu, J. Guo, X. Xie, et al., "GTPase GPN3 Facilitates Cell Proliferation and Migration in Non-Small Cell Lung Cancer by Impeding Clathrin-Mediated Endocytosis of EGFR," *Cell Death Discovery* 11, no. 1 (2025): 38.

6. M. Yadav, A. Sharma, K. Patne, et al., "AXL Signaling in Cancer: From Molecular Insights to Targeted Therapies," *Signal Transduction and Targeted Therapy* 10, no. 1 (2025): 37.

7. T. Soonthonsrima, I. D. Putra, P. Phookphan, Z. Z. Ei, M. Yokoya, and P. Chanvorachote, "A Promising Resveratrol Analogue Suppresses CSCs in Non-Small-Cell Lung Cancer via Inhibition of the ErbB2 Signaling Pathway," *Chemical Research in Toxicology* 38 (2025): 415–432.

8. L. H. Al-Wahaibi, H. A. Abou-Zied, E. A. M. Beshr, B. G. M. Youssif, A. M. Hayallah, and M. Abdel-Aziz, "Design, Synthesis, Antiproliferative Actions, and DFT Studies of New Bis–Pyrazoline Derivatives as Dual EGFR/BRAF^{V600E} Inhibitors," *International Journal of Molecular Sciences* 24, no. 10 (2023): 9104.

9. L. H. Al-Wahaibi, E. M. El-Sheref, M. M. Hammouda, and B. G. M. Youssif, "One-Pot Synthesis of 1-Thia-4-Azaspiro [4.4/5] Alkan-3-Ones via Schiff Base: Design, Synthesis, and Apoptotic Antiproliferative Properties of Dual EGFR/BRAF^{V600E} Inhibitors," *Pharmaceuticals* 16, no. 3 (2023): 467.

10. L. H. Al-Wahaibi, A. M. Gouda, O. F. Abou-Ghadir, et al., "Design and Synthesis of Novel 2,3-Dihydropyrazino [1,2-a] Indole-1,4-Dione Derivatives as Antiproliferative EGFR and BRAFV600E Dual Inhibitors," *Bioorganic Chemistry* 104 (2020): 104260.

11. L. V. Sequist and T. J. Lynch, "EGFR Tyrosine Kinase Inhibitors in Lung Cancer: An Evolving Story," *Annual Review of Medicine* 59, no. 1 (2008): 429–442.

12. Z. Li, W. Zou, J. Yuan, Y. Zhong, and Z. Fu, "Gender Differences in Adverse Events Related to Osimertinib: A Real-World Pharmacovigilance Analysis of FDA Adverse Event Reporting System," *Expert Opinion on Drug Safety* 23, no. 6 (2024): 763–770.

13. Q. Li, B. Li, Q. Wang, C. Wang, M. Yu, and T. Xu, "Marine-Derived EGFR Inhibitors: Novel Compounds Targeting Breast Cancer Growth and Drug Resistance," *Frontiers in Pharmacology* 15 (2024): 1396605.

14. D. Das, L. Xie, and J. Hong, "Next-Generation Egfr Tyrosine Kinase Inhibitors to Overcome C797S Mutation in Non-Small Cell Lung Cancer (2019–2024)," *RSC Medicinal Chemistry* 15 (2024): 3371–3394.

15. X. Shi, X. Wang, W. Yao, et al., "Mechanism Insights and Therapeutic Intervention of Tumor Metastasis: Latest Developments and Perspectives," *Signal Transduction and Targeted Therapy* 9, no. 1 (2024): 192.

16. S. Musa, N. Amara, A. Selawi, et al., "Overcoming Chemoresistance in Cancer: The Promise of Crizotinib," *Cancers* 16, no. 13 (2024): 2479.

17. A. M. Mohamed, O. M. F. Abou-Ghadir, Y. A. Mostafa, K. A. Dahlous, S. Bräse, and B. G. M. Youssif, "Design and Synthesis of New 1,2,4-Oxadiazole/Quinazoline-4-one Hybrids With Antiproliferative Activity as Multitargeted Inhibitors," *Frontiers in Chemistry* 12 (2024): 1447618.

18. B. G. M. Youssif, "Synthesis of a New Series of 4-pyrazolylquinolinones With Apoptotic Antiproliferative Effects as Dual EGFR/BRAFV600E Inhibitors," *RSC Medicinal Chemistry* 15 (2024): 2538–2552.

19. L. Hu, M. Fan, S. Shi, et al., "Dual Target Inhibitors Based on EGFR: Promising Anticancer Agents for the Treatment of Cancers," *European Journal of Medicinal Chemistry* 227 (2022): 113963.

20. H. A. Abou-Zied, E. A. M. Beshr, H. A. M. Gomaa, et al., "Discovery of New Cyanopyridine/Chalcone Hybrids as Dual Inhibitors of EGFR/$BRAF^{V600E}$ With Promising Antiproliferative Properties," *Archiv der Pharmazie* 356, no. 4 (2023): 2200464.

21. L. H. Al-Wahaibi, H. A. Abou-Zied, M. H. Abdelrahman, et al., "Design and Synthesis New Indole-Based Aromatase/iNOS Inhibitors With Apoptotic Antiproliferative Activity," *Frontiers in Chemistry* 12 (2024): 1432920.

22. L. H. Al-Wahaibi, M. A. Mahmoud, Y. A. Mostafa, A. E. Raslan, and B. G. M. Youssif, "Novel Piperine-Carboximidamide Hybrids: Design, Synthesis, and Antiproliferative Activity via a Multi-Targeted Inhibitory Pathway," *Journal of Enzyme Inhibition and Medicinal Chemistry* 38, no. 1 (2023): 376–386.

23. L. H. Al-Wahaibi, A. F. Mohammed, F. E.-Z. S. Abdel Rahman, et al., "Design, Synthesis, Apoptotic, and Antiproliferative Effects of 5-Chloro-3-(2-Methoxyvinyl)-Indole-2-Carboxamides and Pyrido [3,4-b] Indol-1-Ones as Potent $EGFR^{WT}$/$EGFR^{T790M}$ Inhibitors," *Journal of Enzyme Inhibition and Medicinal Chemistry* 38, no. 1 (2023): 2218602.

24. X. Cheng, "A Comprehensive Review of HER2 in Cancer Biology and Therapeutics," *Genes* 15, no. 7 (2024): 903.

25. R. Nussinov, B. R. Yavuz, and H. Jang, "Molecular Principles Underlying Aggressive Cancers," *Signal Transduction and Targeted Therapy* 10, no. 1 (2025): 42.

26. S. Liu, X. Zhang, W. Wang, et al., "Metabolic Reprogramming and Therapeutic Resistance in Primary and Metastatic Breast Cancer," *Molecular Cancer* 23, no. 1 (2024): 261.

27. L. H. Al-Wahaibi, E. M. El-Sheref, H. N. Tawfeek, et al., "Design, Synthesis, and Biological Evaluation of Novel Quinoline-Based EGFR/HER-2 Dual-Target Inhibitors as Potential Anti-Tumor Agents," *RSC Advances* 14, no. 45 (2024): 32978–32991.

28. L. H. Al-Wahaibi, A. M. Mohassab, S. M. Rabea, B. G. M. Youssif, S. Bräse, and E. M. El-Sheref, "Design, Synthesis, and Antiproliferative Activity of New 2-Amino-Pyrano [3,2-c] Quinoline-3-Carbonitriles as Potential EGFR, Braf V600E, and HER-2 Inhibitors," *RSC Advances* 15, no. 45 (2025): 38229–38242.

29. L. H. Al-Wahaibi, H. M. Hafez, F. H. Edrees, H. A. Abou-Zied, B. G. Youssif, and S. Bräse, "Design, Synthesis, and Computational Studies of Novel Pyrazoline-Based Dual EGFR/HER-2 Inhibitors With Apoptotic Antiproliferative Activity," *Journal of Molecular Structure* 1339 (2025): 142364.

30. L. H. Al-Wahaibi, H. A. Abou-Zied, M. Nieger, S. Bräse, B. G. M. Youssif, and H. Tawfik, "Design, Synthesis, Antiproliferative Assessments, and Computational Studies of New quinolin-2 (1H)-Ones as Dual EGFR/HER-2 Inhibitors," *Frontiers in Chemistry* 13 (2025): 1638489.

31. M. M. Morcoss, J. N. Saddik, M. E. Amin, et al., "Design, Synthesis, Antimalarial Activity, and In-Silico Studies of New Benzimidazole/Pyridine Hybrids as Dihydrofolate Reductase Inhibitors," *Bioorganic Chemistry* 156 (2025): 108171.

32. M. J. Akhtar, A. A. Siddiqui, A. A. Khan, et al., "Design, Synthesis, Docking and QSAR Study of Substituted Benzimidazole Linked Oxadiazole as Cytotoxic Agents, EGFR and ERBB2 Receptor Inhibitors," *European Journal of Medicinal Chemistry* 126 (2017): 853–869.

33. F. F. Hagar, S. H. Abbas, H. Gomaa, et al., "Chalcone/1,3,4-Oxadiazole/Benzimidazole Hybrids as Novel Anti-Proliferative Agents Inducing Apoptosis and Inhibiting EGFR & BRAFV(600E)," *BMC Chemistry* 17, no. 1 (2023): 116.

34. S. Jubie, U. Durai, S. Latha, S. Ayyamperumal, A. Wadhwani, and T. Prabha, "Repurposing of Benzimidazole Scaffolds for HER2 Positive Breast Cancer Therapy: An In-Silico Approach," *Current Drug Research Reviews* 13, no. 1 (2021): 73–83.

35. E. A. A. El-Meguid, E. M. M. El-Deen, M. A. Nael, and M. M. Anwar, "Novel Benzimidazole Derivatives as Anti-Cervical Cancer Agents of Potential Multi-Targeting Kinase Inhibitory Activity," *Arabian Journal of Chemistry* 13, no. 12 (2020): 9179–9195.

36. S. Mowafy, A. Galanis, Z. M. Doctor, et al., "Toward Discovery of Mutant EGFR Inhibitors; Design, Synthesis and In Vitro Biological Evaluation of Potent 4-Arylamino-6-Ureido and Thioureido-Quinazoline Derivatives," *Bioorganic & Medicinal Chemistry* 24, no. 16 (2016): 3501–3512.

37. Z. Zhao, H. Wu, L. Wang, et al., "Exploration of Type II Binding Mode: A Privileged Approach for Kinase Inhibitor Focused Drug Discovery?," *ACS Chemical Biology* 9, no. 6 (2014): 1230–1241.

38. P. Furet, G. Caravatti, N. Lydon, et al., "Modelling Study of Protein Kinase Inhibitors: Binding Mode of Staurosporine and Origin of the Selectivity of CGP 52411," *Journal of Computer-Aided Molecular Design* 9 (1995): 465–472.

39. H. E. Hashem, A. E.-G. E. Amr, E. S. Nossier, M. M. Anwar, and E. M. Azmy, "New Benzimidazole-, 1,2,4-Triazole-, and 1,3,5-Triazine-Based Derivatives as Potential EGFRWT and EGFRT790M Inhibitors: Microwave-Assisted Synthesis, Anticancer Evaluation, and Molecular Docking Study," *ACS Omega* 7, no. 8 (2022): 7155–7171.

40. A. Şandor, I. Ionuţ, G. Marc, I. Oniga, D. Eniu, and O. Oniga, "Structure–Activity Relationship Studies Based on Quinazoline Derivatives as EGFR Kinase Inhibitors (2017–Present)," *Pharmaceuticals* 16, no. 4 (2023): 534.

41. P. Bhatia, V. Sharma, O. Alam, et al., "Novel Quinazoline-Based EGFR Kinase Inhibitors: A Review Focussing on SAR and Molecular Docking Studies (2015-2019)," *European Journal of Medicinal Chemistry* 204 (2020): 112640.

42. S. S. Tawfik, A. Hamdi, A. R. Ali, et al., "S-Alkylated Quinazolin-4 (3 H)-Ones as Dual EGFR/VEGFR-2 Kinases Inhibitors: Design, Synthesis, Anticancer Evaluation and Docking Study," *RSC Advances* 14, no. 36 (2024): 26325–26339.

43. H. W. El-Shafey, M. M. Al-Sanea, M. R. Elnagar, et al., "Design and Synthesis of Novel 2-S-Alkylated Quinazolinones as Dual BRAFV600E and EGFR Inhibitors in Melanoma: Mechanistic Insights From Apoptosis and Cell Cycle Modulation," *Bioorganic Chemistry* 161 (2025): 108526.

44. H. M. Abd El-Lateef, M. A. I. Elbastawesy, T. M. Abdelghani Ibrahim, et al., "Design, Synthesis, Docking Study, and Antiproliferative Evaluation of Novel Schiff Base–Benzimidazole Hybrids With VEGFR-2 Inhibitory Activity," *Molecules* 28, no. 2 (2023): 481.

45. T. Al-Warhi, L. S. Alqahtani, G. Alsharif, et al., "Design, Synthesis, and Investigation of Cytotoxic Activity of Cis-Vinylamide-Linked Combretastatin Analogues as Potential Anticancer Agents," *Symmetry* 14, no. 10 (2022): 2088.

46. H. A. M. El-Sherief, B. G. M. Youssif, A. H. Abdelazeem, M. Abdel-Aziz, and H. M. Abdel-Rahman, "Design, Synthesis and Antiproliferative Evaluation of Novel 1,2,4-Triazole/Schiff Base Hybrids With EGFR and B-RAF Inhibitory Activities," *Anti-Cancer Agents in Medicinal Chemistry* 19, no. 5 (2019): 697–706.

47. M. A. Mahmoud, A. F. Mohammed, O. I. A. Salem, S. M. Rabea, and B. G. M. Youssif, "Design, Synthesis, and Antiproliferative Properties of New 1,2,3-Triazole-Carboximidamide Derivatives as Dual EGFR/VEGFR-2 Inhibitors," *Journal of Molecular Structure* 1282 (2023): 135165.

48. A. M. Mohassab, H. A. Hassan, H. A. Abou-Zied, et al., "Design and Synthesis of New Quinoline-Ester/-Amide Derivatives as Potent

Antiproliferative Agent Targeting EGFR and BRAFV600E Kinases," *Journal of Molecular Structure* 1297 (2024): 136953.

49. M. Hisham, H. A. Hassan, H. A. M. Gomaa, B. G. M. Youssif, A. M. Hayalah, and M. Abdel-Aziz, "Design, Synthesis, and Antiproliferative Activity of Quinazolin-4-One/Chalcone Hybrids via the EGFR Inhibition Pathway," *Anti-Cancer Agents in Medicinal Chemistry* 23, no. 17 (2023): 1932–1943.

50. H. A. M. Gomaa, M. E. Shaker, S. I. Alzarea, et al., "Design, Synthesis, and Apoptotic Antiproliferative Efficacy of New Quinazoline/1, 3, 4-Oxadiazole-2-thione Derived EGFR/HER-2 Dual Inhibitors With Anti-Breast Cancer Activity," *RSC Medicinal Chemistry* 16 (2025): 4297–4315.

51. M. A. Mansour, A. M. AboulMagd, S. H. Abbas, M. Abdel-Aziz, and H. M. Abdel-Rahman, "Quinazoline-Chalcone Hybrids as HDAC/EGFR Dual Inhibitors: Design, Synthesis, Mechanistic, and In-Silico Studies of Potential Anticancer Activity Against Multiple Myeloma," *Archiv der Pharmazie* 357, no. 5 (2024): 2300626.

52. J. Stamos, M. X. Sliwkowski, and C. Eigenbrot, "Structure of the Epidermal Growth Factor Receptor Kinase Domain Alone and in Complex With a 4-Anilinoquinazoline Inhibitor," *Journal of Biological Chemistry* 277, no. 48 (2002): 46265–46272.

53. K. Furmanová, O. Vávra, B. Kozlíková, et al., *DockVis: Visual Analysis of Molecular Docking Trajectories, Computer Graphics Forum* (Wiley Online Library, 2020), 452–464.

54. N. M. Habib and M. M. Morcoss, "Various Approaches for Appraisal of the Greenness Profile and Whiteness Assessment of Chromatographic Methods for Determination of Spiramycin, Metronidazole, and Toxic Impurity: Studying In-Silico ADMET Profile of Drug Impurity," *Microchemical Journal* 204 (2024): 110980.

55. M. Janicka, M. Sztanke, and K. Sztanke, "Predicting the Blood-Brain Barrier Permeability of New Drug-Like Compounds via HPLC With Various Stationary Phases," *Molecules* 25, no. 3 (2020): 487.

56. Z. Zhao, L. Xie, and P. E. Bourne, "Structural Insights Into Characterizing Binding Sites in Epidermal Growth Factor Receptor Kinase Mutants," *Journal of Chemical Information and Modeling* 59, no. 1 (2018): 453–462.

57. H. H. Al Sayad, A. A. A. Abdul Sahib, and Z. K. Oleiwi, "Molecular Docking Study of Five Novel 1,2,3-Triazole Linked Metronidazole Derivatives as Cytotoxic Agents," *Karbala Journal of Pharmaceutical Sciences* 15, no. 24 (2024): 70–84.

Supporting Information

Additional supporting information can be found online in the Supporting Information section.
Supplementary Data. Appendix A.